Existential Uncertainty of Spatial Objects Segmented From Satellite Sensor Imagery

Arko Lucieer and Alfred Stein

Abstract—This research addresses existential uncertainty of spatial objects derived from satellite sensor imagery. An image segmentation technique is applied at various values of splitting and merging thresholds. We test the hypothesis that objects occurring at many segmentation steps have less existential uncertainty than those occurring at only a few steps.

Index Terms—Existential uncertainty, satellite sensor imagery, segmentation, spatial objects, visualization.

I. INTRODUCTION

Object-oriented approaches to satellite sensor image processing become increasingly popular with the growing amount of high-resolution satellite imagery. Segmentation techniques can help to extract spatial objects from an image scene. Uncertainty will be present in any segmented image and can have a significant effect on further image processing steps. Therefore, existential uncertainty is of a major importance for spatial objects, expressing the uncertainty that an object, as identified by a segmentation procedure, exists [1].

Image segmentation is primarily used to subdivide an image into different segments. These segments may or may not correspond to objects as observed in the terrain. Image segmentation is in a sense related to spectral classification, which puts pixels into classes defined either *a priori* or during classification. Segmentation differs from classification, however, as spatial contiguity is an explicit goal of segmentation, whereas it is only implicit in classification. Spectral classification of satellite sensor images applied on a pixel basis ignores potentially useful spatial information between pixels. Whereas image classification has become a routinely applied method, image segmentation never became very popular in earth observation applications. The main reason is that the spatial resolution of satellite sensor imagery is a prime limiting factor for segmentation [2]. Increasing availability of high-resolution satellite sensor imagery, such as acquired by the IKONOS satellite, however, requires additional attention to uncertainty in segmentation procedures.

Quantification of existential uncertainty is essential to evaluate segmentation quality. Recently, probabilistic and fuzzy techniques have been used to quantify and model uncertainty in classification procedures [2], [3]. This has mainly been applied on a pixel basis, and no attention has been given to uncertainty related to image objects.

An essential step in image segmentation is its validation. The existence of objects, however, depends on the context of a study: for example, topographical objects may differ from geological objects or land cover objects. In this study, we take the approach that an object with a high existential certainty corresponds to an object as represented on a topographic map.

Besides quantification, visualization is important to communicate uncertainty [4], [5]. Visualization allows the user to explore uncertainty in spatial data [6], e.g., by animation or by linked views, and to review effects of changing parameters during segmentation.

The objective of this research is to quantify and visualize existential uncertainty of spatial objects derived from high-resolution satellite sensor imagery with a split-and-merge image segmentation algorithm. The study is applied on an IKONOS image of an agricultural area near Enschede, The Netherlands. A topographic map is used to validate segmentation results.

II. METHODS

A. Image Segmentation Using a Split-and-Merge Algorithm

Commonly, three approaches are distinguished toward segmentation: edge-based segmentation, region-based segmentation, and split-and-merge segmentation [7]. Split-and-merge segmentation, as applied in this study, consists of a region-splitting phase and an agglomerative clustering phase. In the splitting phase, the image B is initially considered as a square block of pixel values with mean vector M_B and covariance matrix S_B. The dimension is determined by the number of bands in the image; in case of IKONOS this equals four. This block is split into four square subblocks (B_1, B_2, B_3, and B_4), characterized by vectors of mean pixel values M_{B_1}, M_{B_2}, M_{B_3}, and M_{B_4} and covariance matrices S_{B_1}, S_{B_2}, S_{B_3}, and S_{B_4} in the subblocks. To define homogeneity, we consider a threshold ϵ_{ms} for the mean and thresholds ϵ_{ss} for the covariance matrix. These values are chosen in advance and kept constant during segmentation. An image block B is homogeneous if

$$|M_{B_i} - M_B| < \epsilon_{ms}, \qquad \text{for } i = 1, 2, 3, 4 \tag{1}$$

and

$$|S_{B_i} - S_B| < \epsilon_{ss}, \qquad \text{for } i = 1, 2, 3, 4 \tag{2}$$

and heterogeneous if one of these equations does not apply. Heterogeneous subblocks are split recursively until homogeneity occurs or until a minimum block size of one pixel is reached. The resulting data structure is a regular quadtree. In the clustering phase, adjacent block segments are merged if the combined segment is homogeneous. The homogeneity rules (1) and (2) are applied in a similar way. Thresholds for mean and covariance matrix are denoted by ϵ_{mm} and ϵ_{sm}, respectively [8].

B. Quantifying Existential Object Uncertainty

The final result of a segmentation procedure depends upon the thresholds ϵ_{ms}, ϵ_{ss}, ϵ_{mm}, and ϵ_{sm}. For various thresholds, objects of different size emerge. Small ϵ values lead to small objects, whereas large values result in large objects. Some objects are insensitive to threshold values, whereas some objects disappear beyond a particular threshold and others expand in size. We hypothesize that objects emerging in a uniform shape irrespective of threshold values correspond to real-world objects as represented on a topographic map. Objects disappearing at a specific threshold have a high degree of existential uncertainty and are called "unstable objects." Objects that remain the same at different segmentation levels are "stable" objects and have a low degree of existential uncertainty.

To quantify existential uncertainty in a segmentation procedure, ranges for the splitting thresholds ϵ_{ms} and ϵ_{ss} and merging thresholds ϵ_{mm} and ϵ_{sm} are chosen. These ranges are divided into n steps. At each step, object boundaries, in the form of segment edge pixels, are determined. At step k, these boundary pixels are assigned the value one and nonboundary pixels the value zero and are represented on

a segment–boundary image I_k. This results in a boundary stability image (BSI), defined as

$$\text{BSI} = \frac{\sum_{k=0}^{n} I_k}{n}. \tag{3}$$

A BSI has values between 0.0 and 1.0, the value 0.0 emerging in the absence of a boundary at each step, the value 1.0 in the presence of a boundary at each step, and intermediate values in between. Segment boundaries with large BSI values are boundaries with a high existential certainty, and small BSI values represent boundaries with high existential uncertainty.

C. Visualization of the Existential Uncertainty of Objects

Correct interpretation of uncertainty information depends largely on communication from system to user. Several visualization techniques can be used to depict existential uncertainty of segmented image objects. For visualizing uncertainty of object boundaries, a continuous gray scale or a color scale can be used. According to Blenkinsop *et al.* [5], grayscale images are most effective in communicating uncertainty. In addition, dynamic linking and geographic brushing functionalities can help to increase perception of uncertainty. Uncertainty values are obtained from the image by dynamically linking the uncertainty image and the original image with a data window. The data window displays the coordinates, reflection value, and uncertainty value of a pixel at the cursor location. Relations between original reflection values and related segments can be explored in this way.

D. Segmentation Validation

Segmentation validation is necessary to assess segmentation accuracy. To quantitatively assess a segmentation result, we identify m objects from a reference dataset and calculate the percentage of overlap of the largest segments inside these objects. The image is oversegmented if overlap is less than 100% and undersegmented if overlap is more than 100%. To quantify the fit of each of the reference objects with the largest segments overlapping these objects, we use the area fit index (AFI)

$$\text{AFI} = \frac{A_{\text{reference object}} - A_{\text{largest segment}}}{A_{\text{reference object}}} \tag{4}$$

where A is the area in pixels. For a perfect fit, the overlap is 100% and $\text{AFI} = 0.0$. A reference object is oversegmented if the overlap is less than 100% and $\text{AFI} > 0.0$. A reference object is undersegmented if the overlap is 100% and $\text{AFI} < 0.0$. In some situations, overlap can be less than 100% and $\text{AFI} < 0.0$; then the object is oversegmented, but the largest segment is larger than the reference object.

Another technique for segmentation validation is to quantitatively compare segment boundaries with boundaries on a reference map. Following Delves *et al.* [9], let p be a boundary pixel of a region in the reference map and $D(p)$ be the shortest (Euclidian) distance, measured in pixels, between p and any boundary pixel in the segmented image. Then

$$D(b) = \frac{\sum_{\text{boundary pixels}} D(p)}{N} \tag{5}$$

where the sum is taken over all boundary pixels in region b, and N is the number of boundary pixels in the reference dataset. As such, $D(b)$ measures the average distance between a segment boundary pixel and the reference boundary. For a perfect fit, $D(b) = 0$. If the region b equals the whole image, the image segmentation accuracy measure is obtained, denoted by $D(B)$. The number of boundary pixels in the segmented image M, however, is not taken into account. For high values

of M, many boundary pixels in the neighborhood of p occur, and therefore, low $D(B)$ values are obtained. A boundary image with a high M value may be extremely oversegmented. To correct for M in the calculation of $D(B)$, we propose the following correction factor

$$D(B)_{\text{corr}} = \frac{|N - M|}{N} + D(B). \tag{6}$$

III. STUDY AREA

The study area, characterized by agriculture, is located southwest of Enschede, The Netherlands. Six land cover types occur in the area: water, grassland, woodland, bare soil, cereals, and buildup area. Both homogeneous and heterogeneous parcels occur, with crisp objects dominating the region. A subset of 512×512 pixels of an IKONOS image, covering all major land cover types, acquired on April 3, 2000 is used in this study [Fig. 1(a)].

A vector-based topographic map on scale 1 : 10 000 is used as a reference dataset for segmentation validation. The vector map is converted to raster format with a spatial resolution equal to the IKONOS image. The image is geometrically corrected with ground control points derived from the topographic map. The root-mean-squared error (RMSE) of geometric correction is 0.349 pixels. A first-degree polynomial function is used to register the image to the topographic map coordinate system.

IV. RESULTS

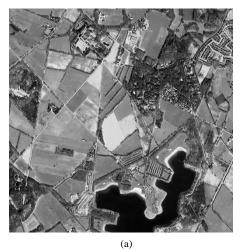### A. Quantification and Visualization of Existential Uncertainty

Fig. 1(b) presents a single segmentation of the image. In this segmentation, the following values are used: $\epsilon_{ms} = 10.0$, $\epsilon_{ss} = 300.0$, $\epsilon_{mm} = 20.0$, and $\epsilon_{sm} = 100.0$. In the splitting phase, 60 355 homogeneous blocks are formed. After merging, 18 387 objects remain. Forested areas and urban regions contain a large number of very small segments, caused by the large variance in reflection in these areas. Homogeneous parcels and the water body are correctly segmented, whereas heterogeneous parcels are oversegmented.
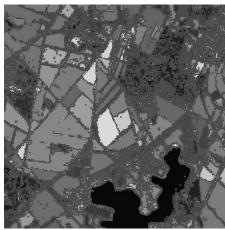
As crisp objects dominate the image scene, we assume that objects can be represented by their boundaries, and we calculate the boundary stability image BSI. The number of segmentation steps n is 100. Thresholds for splitting are kept small $\epsilon_{ms} = 10.0$ and $\epsilon_{ss} = 300.0$ and are kept constant for all steps to avoid blocky artifacts in the segmentation result. Thresholds for merging range from $\epsilon_{mm} = 12.0$ to 42.0 and $\epsilon_{sm} = 25.0$ to 275.0. Fig. 1(c) shows the resulting BSI in gray scale. Bright values depict high boundary stability, while low stability is represented by darker values; nonboundary pixels are black. Boundaries of heterogenous parcels and boundaries of small objects in urban and forested areas are characterized by low stability and, therefore, high uncertainty values. Boundaries of the water body, homogeneous parcels, and roads can be clearly identified in the image and are depicted by high BSI values.

B. Segmentation Validation

The first step in segmentation validation is a visual comparison of object boundaries from a segmentation result with object boundaries from the topographic reference map. Again, dynamic linking can help to explore similarities and discrepancies between the two maps. To quantitatively assess segmentation results, we have taken seven reference objects from the topographic raster map. These objects represent the land cover in the study area (Table I).

To quantify the goodness-of-fit of a segmentation with the reference objects, we calculate the AFI [see (4)]. AFI values for the seven reference objects for all segmentation steps are presented in Fig. 2. Object
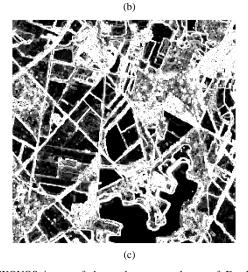
(a)

(b)

(c)

Fig. 1. IKONOS image of the study area southwest of Enschede, The Netherlands (acquired April 3, 2000).

TABLE I
DESCRIPTION OF THE REFERENCE OBJECTS USED IN VALIDATION

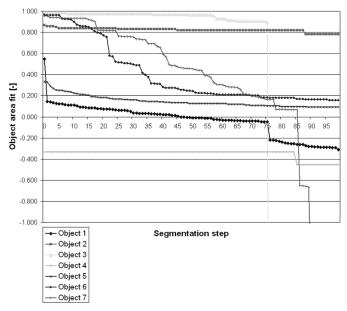| Object	Area [pixels]	Description
object 1	16453	Water body (lake)
object 2	421	Recreational beach
object 3	560	Road
object 4	33	Building
object 5	1540	Homogeneous crop parcel
object 6	2101	Heterogeneous crop parcel
object 7	2823	Forest patch

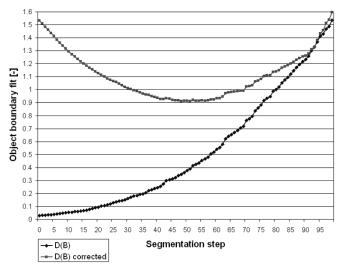Fig. 2. AFI values for each reference object for each segmentation step.

Fig. 3. Boundary fit $D(B)$ and $D(B)_{\mathrm{corr}}$ values for the whole image for each segmentation step.

1 reaches $\mathrm{AFI} = 0.0$ at segmentation step 50; its overlap is 96% at this step. Objects 2 and 3 do not reach an AFI of 0.0. Object 2 is oversegmented for all steps. At segmentation step 76, the largest segment of object 3 is merged with an agricultural parcel, resulting in a large negative AFI value. Object 4 has a negative AFI value, between -0.36 and -0.44, for each step. Thus, the largest segment is larger than the reference object (undersegmented), but does not entirely overlap (maximum overlap = 82%). Segmentation of object 5 is best at the final segmentation step (overlap is 90% and $\mathrm{AFI} = 0.10$). The same holds for object

6, but overlap is 83% and $\mathrm{AFI} = 0.17$. Object 7 is best segmented when $\mathrm{AFI} = 0.08$, and overlap is 82% at step 85. After segmentation step 86, object 7 is undersegmented.

Segmentation validation for the whole image is carried out using a boundary-matching procedure. We use the measure $D(B)$ [from (5)] to describe a segment's fit to a reference object by means of its boundaries. Thus, all boundaries from each segmentation step are compared to the boundaries of objects in the topographic reference map. $D(B)$ values in Fig. 3 show that the best fit of segment boundaries is obtained

at the first segmentation step. Most objects, however, are severely over-segmented in the first step. Therefore, a corrected value $D(B)_{\text{corr}}$ [see (6)] is applied to correct for the number of boundary pixels in the segmented image. Where $D(B)_{\text{corr}}$ equals $D(B)$, the number of boundary pixels is equal in both the segmented image and topographic map, and the correction factor is 1.0. At this step, $D(B) = 1.33$. $D(B)_{\text{corr}}$ values show that an optimal segmentation result, for a best boundary fit and an optimal number of boundary pixels, is obtained at segmentation step 55; here $D(B)_{\text{corr}} = 0.91$.

V. DISCUSSION

The split-and-merge algorithm used in this study generally produces good segmentation results. Glasbey [10] found that boundaries, derived this way, are rough and retain some of the artifacts of blocks from the splitting phase. If the thresholds for splitting are kept small, however, these blocky artifacts are no longer present in the final segmentation result. Texture measures could be used to improve segmentation in texture-rich areas such as the forested and urban regions in the IKONOS image. Long-shaped objects (e.g., objects 2 and 3) give difficulties in segmentation. This can be explained by the fact that neighbor adjacency is calculated in four directions (north, east, south, west), called a four-adjacency model. The eight-adjacency model takes into account the diagonal neighbors as well. This adjacency model might be useful in segmenting long-shaped objects with a diagonal orientation, like objects 2 and 3. Undersegmentation of small objects, like object 4, can be explained by the fact that the spatial resolution of the multispectral IKONOS bands is too coarse for detection of these small objects. Incorporation of information from the panchromatic band could be helpful in this case.

In this study, existential uncertainty of image objects is discussed. Other types of uncertainty, like extensional uncertainty, can be distinguished as well [1], [11]. This type of uncertainty refers to the uncertainty in spatial extent of an object. Extensional uncertainty is important for the spatial representation of fuzzy objects. For a crisp object, existential uncertainty plays the most important role. The context of the validation map is also an important issue. Topographic objects used as reference are likely to give other segmentation accuracy values as objects derived from a soil map, vegetation map, or geological map.

VI. CONCLUSION

In this communication, we propose a method to quantify and visualize existential uncertainty of spatial objects derived from satellite sensor imagery with a split-and-merge image segmentation algorithm. Objects disappearing at a specific segmentation threshold have a high degree of existential uncertainty and are called "unstable objects." Objects that remain the same at different segmentation levels are "stable" objects and have a low degree of existential uncertainty. Existential uncertainty is characterized by the boundary stability image BSI derived from a range of segmentations generated with different threshold values. Seven reference objects on a topographic map have been selected for segmentation validation. The percentage of overlap and the area fit index AFI are measures used to quantify segmentation accuracy for these objects. To determine segmentation accuracy for the whole image, segment boundaries are used to calculate the fit $D(B)$ with the topographic boundaries. We have used a correction factor $D(B)_{\text{corr}}$ to correct for the number of boundary pixels in the segmented image. We conclude that the boundary stability index (BSI) allows a quantification of existential uncertainty and is suitable for its visualization. The area fit index (AFI) and the corrected boundary fit index $(D(B)_{\text{corr}})$ are suitable measures for validation of segmentation results.

REFERENCES

[1] M. Molenaar, *An Introduction to the Theory of Spatial Object Modeling for GIS*.   New York: Taylor & Francis, 1998.

[2] B. H. H. Gorte and A. Stein, "Bayesian classification and class area estimation of satellite images using stratification," *IEEE Trans. Geosci. Remote Sensing*, vol. 36, pp. 803–812, May 1998.

[3] J. Zhang and G. M. Foody, "Fully-fuzzy supervised classification of suburban land cover from remotely sensed imagery: Statistical and artificial neural network approaches," *Int. J. Remote Sens.*, vol. 22, no. 4, pp. 615–628, 2001.

[4] F. J. M. van der Wel, L. C. van der Gaag, and B. G. H. Gorte, "Visual exploration of uncertainty in remote sensing classification," *Comput. Geosci.*, vol. 24, no. 4, pp. 335–343, 1997.

[5] S. Blenkinsop, P. F. Fisher, L. Bastin, and J. Wood, "Evaluating the perception of uncertainty in alternative visualization strategies," *Cartographica*, vol. 37, no. 1, pp. 1–13, 2000.

[6] A. M. MacEachren and M. J. Kraak, "Research challenges in geovisualization," *Cartography Geograph. Inform. Syst.*, vol. 28, no. 1, pp. 3–12, 2001.

[7] R. M. Haralick and L. G. Shapiro, "Image segmentation techniques," *Comput. Vis., Graph. Image Process.*, vol. 29, no. 1, pp. 100–132, 1985.

[8] D. K. Panjwani and G. Healey, "Markov random field models for unsupervised segmentation of textured color images," *IEEE Trans. Pattern Anal. Machine Intell.*, vol. 17, pp. 939–954, Oct. 1995.

[9] L. M. Delves, R. Wilkinson, C. J. Oliver, and R. G. White, "Comparing the performance of SAR image segmentation algorithms," *Int. J. Remote Sens.*, vol. 13, no. 11, pp. 2121–2149, 1992.

[10] C. A. Glasbey and G. W. Horgan, *Image Analysis for the Biological Sciences*.   New York: Wiley, 1995.

[11] T. Cheng and M. Molenaar, "Formalizing fuzzy objects from uncertain classification results," *Int. J. Geograph. Inform. Sci.*, vol. 15, no. 1, pp. 27–42, 2001.